JOURNAL OF MATERIALS SCIENCE 13 (1978) 657–665

The identification of saucer-pit (S-pit) defects in GaAs

D. J. STIRLAND, P. D. AUGUSTUS
Allen Clark Research Centre, The Plessey Company Limited, Caswell, Towcester, Northants, UK

B. W. STRAUGHAN
R.S.R.E. (Malvern), St. Andrews Road, Malvern, Worcs, UK

Samples of gallium arsenide from liquid encapsulated Czochralski grown ingots, doped with either tellurium or selenium to carrier concentrations $\sim 10^{18}$ cm^{-3} revealed shallow pits (S-pits) by etching. Although the S-pits were randomly distributed throughout the matrix, areas of high densities were associated with dislocations. This observation was utilized to identify the types of defects which became S-pits when etched. Transmission electron microscope specimens of etched material were examined in the dislocation regions, and showed directly that faulted loops with Frank partials $\mathbf{b} = 1/3a_0 \langle 1\,1\,1 \rangle$ containing precipitate particles could become S-pits. It was further deduced from the combined optical and electron microscope observations that both faulted $\{1\,1\,1\}$ and unfaulted $\{1\,1\,0\}$ dislocation loops became S-pits provided they contained precipitate partices.

1. Introduction

It is possible that the first occurrence of the nomenclature "saucer-pit" is to be found in a paper by Lyon in 1963 [1]. This described how the variability of reverse bias characteristics in germanium p–n–p alloy junction transistors could be correlated with variations in the number density of shallow etch pits, termed saucers, produced when the $\{1\,1\,1\}$Ge surfaces were etched. Lyon emphasized that these shallow pits were entirely different from dislocation etch pits and suggested that they were due to point defects, such as clusters or precipitated impurities. This explanation was at variance with those put forward by earlier investigators of $\{1\,1\,1\}$ germanium such as Rosi [2], who suggested that the shallow pits might be due to mixed dislocations, and Tweet [3], who proposed that the pits were formed by etching vacancy aggregates. A recent publication by Pearce and McMahon [4] has demonstrated that metallic contamination prior to or during epitaxial growth of $\{0\,0\,1\}$ silicon layers is responsible for the formation of microdefects in the form of dislocation loops, which are transformed into saucer, or S-pits, by Secco etching [5].

The first report of "numerous fine etch pits, differing from dislocation etch pits" for a compound semiconductor was given by Iizuka [6], for $\{1\,1\,1\}$Ga and $\{1\,1\,1\}$As etched surfaces of heavily Te-doped GaAs, i.e. carrier concentrations of 1.6×10^{18} and 6.4×10^{18} cm^{-3}. He conjectured that the fine pits were associated with the strain fields of microprecipitates of Te, or Te-rich complexes. Subsequently [7] he reported that clusters of small, shallow, flat-bottomed etch pits could be produced by the use of suitable etchants on the $\{1\,1\,1\}$P and the $\{1\,1\,0\}$ cleavage faces of GaP crystals containing S or Te dopants. Rozgonyi and Afromowitz [8] and Rozgonyi *et al.* [9] showed how reductions in photoluminescence efficiencies of certain GaP diodes could be related to the presence of high concentrations of those defects which, after a suitable etch treatment, become shallow, flat-bottomed pits. The latter authors used the term saucer-pits (S-pits) to described these pits. Stirland and Straughan [10] adopted

© *1978 Chapman and Hall Ltd. Printed in Great Britain.*

the same nomenclature to designate small pits produced by etching Te and Se doped GaAs specimens with {0 0 1} surface orientation.

The work described here is an attempt to determine precisely the nature of the faults which develop into S-pits in doped GaAs {0 0 1} orientation specimens after suitable etching.

2. Experimental

2.1. Specimen description and preparation

The majority of samples employed in this study consisted of single crystal wafers cut from liquid encapsulated Czochralski (LEC) grown ingots, doped with either Te or Se to give n-type GaAs with carrier concentrations of 0.7×10^{18} to 1.5×10^{18} cm^{-3}. Since the quoted carrier concentration figures are obtained from electrical measurements they represent minimum total dopant concentrations. The wafer surfaces were cut 2° off {0 0 1} orientation towards the nearest {1 1 0}. After lapping, the surfaces were treated with 3:1:1, H_2SO_4:H_2O_2:H_2O [11] for 15 min at 45° C to remove all traces of preparative work damage. Silicon-doped Bridgman grown specimens with carrier concentrations ranging from 1.0×10^{18} to 4×10^{18} cm^{-3} were prepared in a similar way.

Specimens for optical examination were etched in the Abrahams and Buiocchi [12] A/B etch for a wide range of times at room temperature, and subsequently examined by Nomarski [13] interference contrast. A useful method was the repeated etching and micrography of identical areas, in order to establish how particular features changed with etching time. A number of samples were etched in molten KOH at 300° C, as described by Grabmaier and Watson [14].

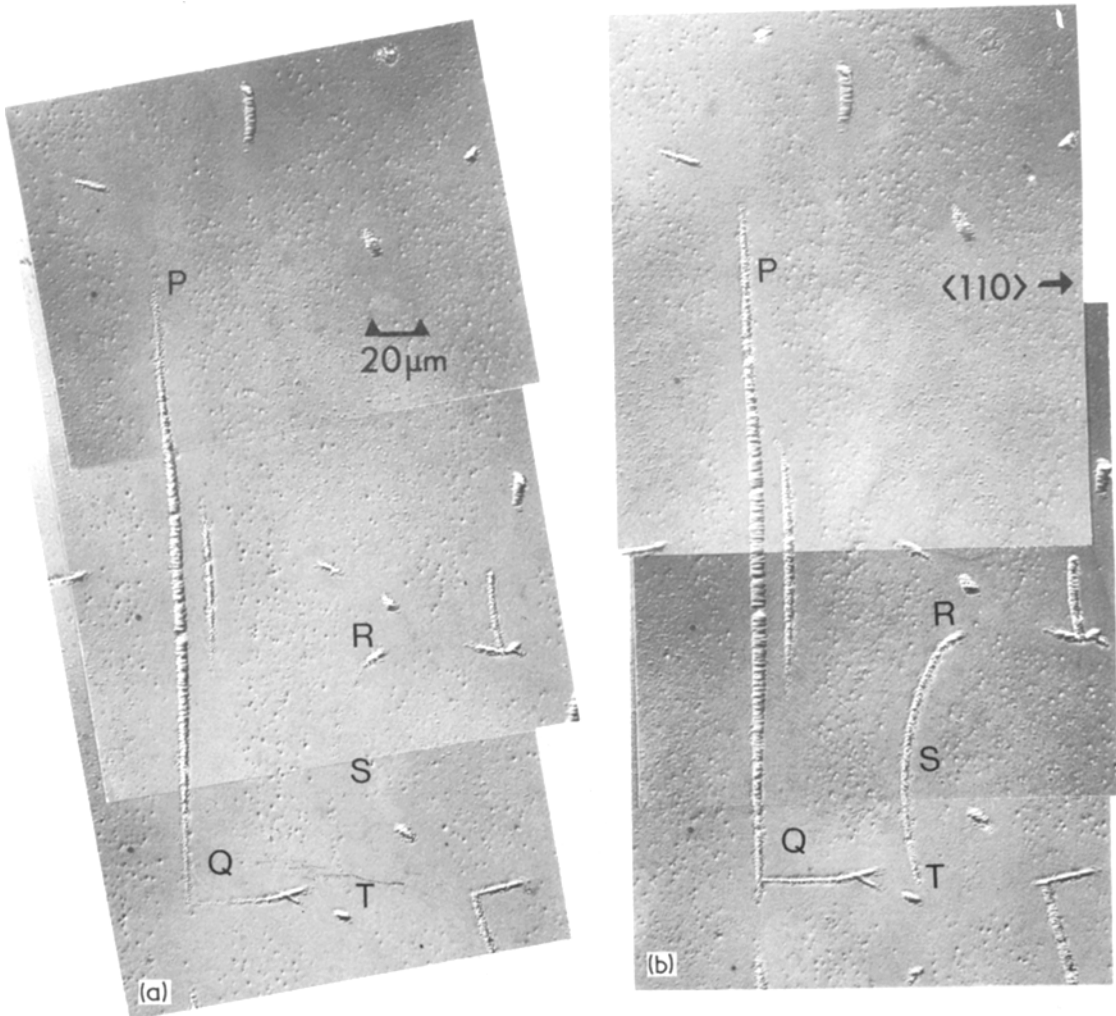

Figure 1 {0 0 1} Te-doped GaAs (carrier concentration ~ 1×10^{18} cm^{-3}) Nomarski interference contrast micrographs. (a) Dislocation structure after 85 sec A/B etch (b) Dislocation structure after 115 sec A/B etch.

Specimens for transmission electron microscopy (TEM) examination were prepared by cutting ultrasonically 2 mm diameter discs either from substrates which had been treated in 3:1:1, $H_2SO_4:H_2O_2:H_2O$ only, or from fragments which had been A/B etched after this treatment. The discs were lapped from the back surface to a thickness of $\sim 120\,\mu m$ and then jet-thinned from the same side in a stream of chlorine dissolved in methanol [15]. TEM samples were examined in a conventional 100 kV microscope, and in some instances in a high voltage microscope (HVEM) at 500 kV.

2.2. Optical microscopy results

Te- and Se-doped {0 0 1}GaAs substrates with carrier concentrations of $1.0 \times 10^{18}\,cm^{-3}$ behaved in a similar manner when etched with the A/B solution. This behaviour is typified by the series of micrographs which comprise Figs. 1 to 3. The etched surfaces exhibited linear features such as PQ and RST in Figs. 1a and b which subsequent examination by other methods such as electron microscropy and X-ray topography have identified as being associated with dislocations [16]. These linear features consisted of lines of densely packed ($\sim 2 \times 10^8\,cm^{-2}$) shallow pits with diameters ~ 0.5 to $1.0\,\mu m$. Flanking these linear features were regions $\sim 20\,\mu m$ wide which appeared devoid of any etch features. Beyond these denuded areas, and remote from the dislocations, was a matrix region which contained both shallow etch pits similar to those delineating the dislocations, and etch ridges or mounds. The shallow pits and ridges occurred at densities $\sim 5 \times 10^6\,cm^{-2}$. The inception, growth, and decay of these features was studied by repeated etching and micrography and Figs. 2 and 3 illustrate typical results.

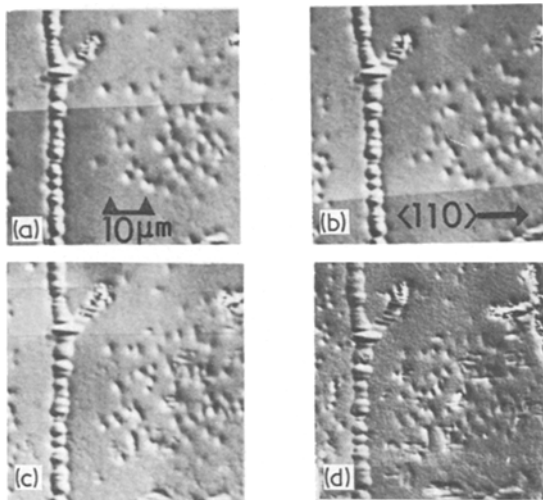

Figure 2 Growth and decay of etch ridges after (a) 5.0 min, (b) 5.5 min, (c) 6.25 min and (d) 7.6 min A/B etch.

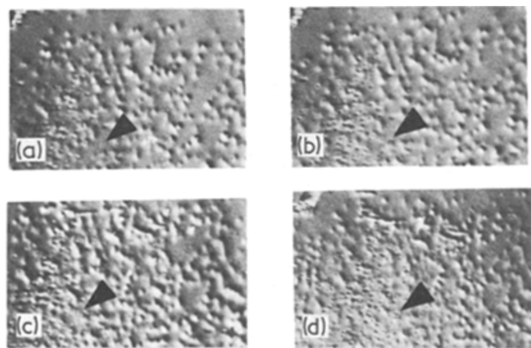

Figure 3 Growth and decay of S-pits after (a) 5.0 min, (b) 5.5 min, (c) 6.25 min, and (d) 7.0 min A/B etch. The marker indicates the same point on each micrograph. Identical orientation to Fig. 2.

All the statements given above concerning the topology of the various etch features (i.e. shallow pits and ridges) have been confirmed by three different methods. Firstly, calibration specimens with known features were employed in the interference contrast microscopy in order to ensure that raised or depressed features could be identified unambiguously. Secondly, etched samples were examined in the scanning electron microscope (SEM). This method established that the pits were indeed shallow depressions, because it was necessary to tilt the specimens so that the incident electron beam fell at $\sim 10^\circ$ to the etched surface in order to produce good contrast images of the pits [17]. Thirdly, platinum-carbon replicas prepared by shadowing etched surfaces at 10° grazing incidence were examined by TEM. Pit depth estimates of $\sim 1/20 \times$ (the pit diameter) were found: thus pits $\sim 1\,\mu m$ diameter had their centres ~ 500 Å below the surrounding matrix level.

The shallow pits are the etch features which have been called saucer- or S-pits by Stirland and Straughan [10]. The remainder of this work will describe how those defects which become S-pits when attacked by the A/B etchant have been located and identified. In principle, it was only necessary to find individual S-pits at which the defects were still present in large enough proportions to be identified by TEM techniques. In practice, the method made use of the observation that the shallow pits seen in the matrix regions of Figs. 1a, 1b and 3 which have previously been named as S-pits, are identical with the shallow pits

which delineate the dislocations. Because the latter occur at greater densities than the former, there is a greater probability of locating appropriately sited defects for correlation with pit features at dislocations, than in the matrix material.

Careful examination of the S-pits at the dislocations PQ and RST in Figs. 1a and 1b and the isolated S-pits of Fig. 3 showed that the initial appearance of each S-pit was a shallow circular depression $\sim 0.5\,\mu m$ diameter. With continued etch attack, the pits elongated in one specific $\langle 1\,1\,0 \rangle$ direction to become elliptic in shape. In contrast, the etch ridges (Fig. 2) elongated either in $[1\,1\,0]$ or in $[1\,\bar{1}\,0]$ directions, as etching was continued.

The change of shape of S-pits surrounding a dislocation with etching time meant that positions of various parts of dislocations relative to the original surface could be deduced. For example in Fig. 1a the etch had just exposed the top (P) and bottom (Q) portions of the marked dislocation, whereas the central section had been attacked long enough for the pits to have elongated. After further etching (Fig. 1b) the circular pits at P and Q became elliptic in turn. The dislocation arc RST in Fig. 1b had developed into a close packed mass of S-pits from a few isolated S-pits, demonstrating that this section of dislocation originally lay nearly parallel with, and below, the initial surface of Fig. 1a.

Similar specimens were etched in molten KOH at 300° C [14]. This is an "orthodox" etch, in that etch pits consisting of six-sided terraced pits were produced at the sites of emergent dislocations, rather than linear features. However, saucer-pits were found in the matrix regions remote from the dislocation pits, indicating that this etching behaviour is not solely a function of the A/B etchant.

2.3. Transmission electron microscopy results

A number of different disc specimens of Te- and Se-doped GaAs substrates were examined by conventional (100 kV) TEM and by (500 kV) HVEM, the latter enabling regions around 1.0 to 1.5 μm thickness to be studied. It was found that practically all of the dislocations observed were similar to one or other of the two dislocation shown in Fig. 4, and a few exhibited characteristics of both. Essentially, one dislocation in Fig. 4 was straight and the other was helical, and because both dislocations could be seen over a distance of 30 μm they lay essentially parallel to the $\{0\,0\,1\}$ surface. Some of the helical turns appeared to have pinched-off to become separate loops. Both dislocations had predominantly edge character with $\mathbf{b} = \frac{1}{2} a_0 \langle 1\,1\,0 \rangle$. Lying in roughly cylindrical sheaths round each dislocation could be seen collections of dislocation loops. Round the helical dislocation the loops were prismatic, with $\mathbf{b} = \frac{1}{2} a_0 \langle 1\,1\,0 \rangle$, and lay on $\{1\,1\,0\}$ planes. Typical loop diameters had values of a few hundred Angstroms. It has not yet been determined whether they were of vacancy or interstitial nature. Similar prismatic $\{1\,1\,0\}$ loops were present around the straight dislocation but at a much smaller concentration. The predominating defects in this region were faulted loops lying on $\{1\,1\,1\}$ planes. Analysis by standard procedures [18] showed that the loops were extrinsic, i.e. equivalent to the insertion of an extra $\{1\,1\,1\}$ disc of material into the matrix. Each loop was bounded by an edge dislocation, a Frank partial with $\mathbf{b}_F = \frac{1}{3} a_0 \langle 1\,1\,1 \rangle$. Loop diameters ranged from ~ 700 to 2500 Å.

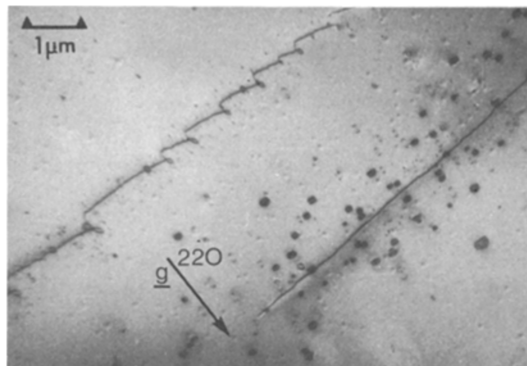

Figure 4 $\{0\,0\,1\}$ Te-doped GaAs (carrier concentration $\sim 1 \times 10^{18}\,cm^{-3}$) HVEM transmission micrograph.

Some properties of the $\{1\,1\,1\}$ loops are demonstrated by the micrographs of Fig. 5. By choice of appropriate 220 type reflections the stacking fault contrast could be removed ($\mathbf{g} \cdot \mathbf{R} = n$ ($n =$ integer) [19]). In this configuration one or more small "precipitate" particles could be seen attached to the dislocation loops. Some complex arrangements consisted of overlapping loops, and in these cases particles lying inside the outermost loop circumference could be observed. An example is shown in Fig. 5, together with single $\{1\,1\,1\}$ loops containing particles. "Precipitate" particles were also found at some perfect dislocation loops as shown arrowed in Fig. 6. These loops often appeared to have been pinched off from the line

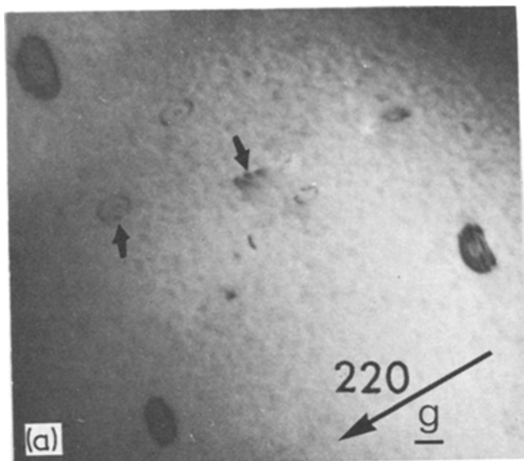

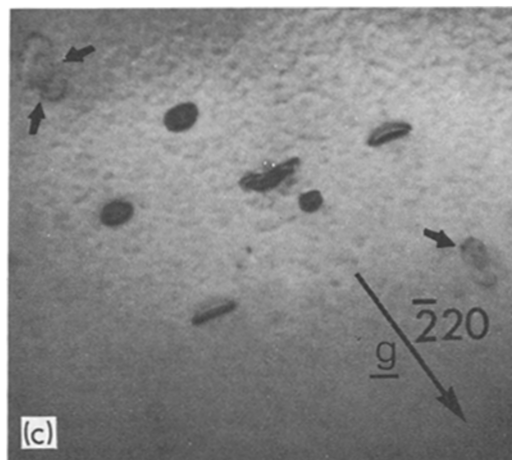

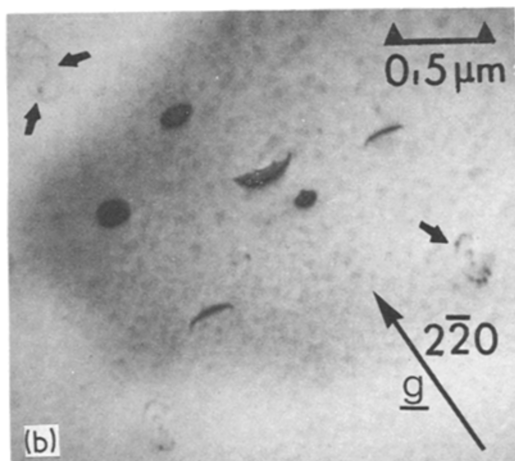

Figure 5 "Precipitate" particles (arrowed) at {1 1 1} loops, visible when stacking fault contrast is removed by appropriate reflection g.

dislocation. The tiny prismatic {1 1 0} loops around the helical dislocation in Fig. 4 were too small to determine whether particles were present or not.

All the characteristics of the various loop defects were determined from observations made on areas containing dislocations. In contrast, areas remote from dislocations contained very few loops. The discrepancy between the optical observations (e.g. Fig. 1) and the TEM observations will be considered in Section 3.1.

2.4. TEM observations of A/B etched specimens

The most informative micrographs were given by specimens which first had been A/B etched on a chemically polished (3:1:1; H_2SO_4:H_2O_2:H_2O) surface and then made thin enough for TEM by a jet of chlorinated methanol applied at the opposite surface. Fig. 7 shows an example: this specimen was a Te-doped GaAs sample etched for 90 sec in the A/B solution prior to thinning for TEM examination. The arrowed features A, B, and C represent S-pits, which were seen in transmission as nearly circular, thin regions of the specimen. Examination of pit A showed that approximately one half of a {1 1 1} loop containing a "precipitate" particle was present. Pit B contained a smaller fragment of a

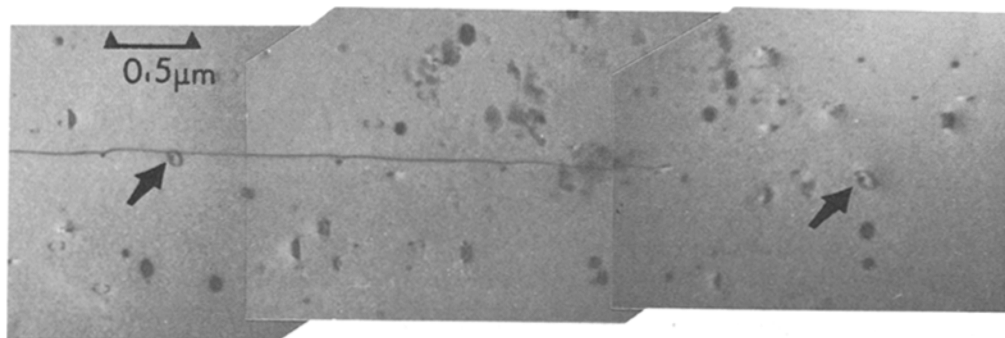

Figure 6 "Precipitate" particles (arrowed) at {1 1 0} loops.

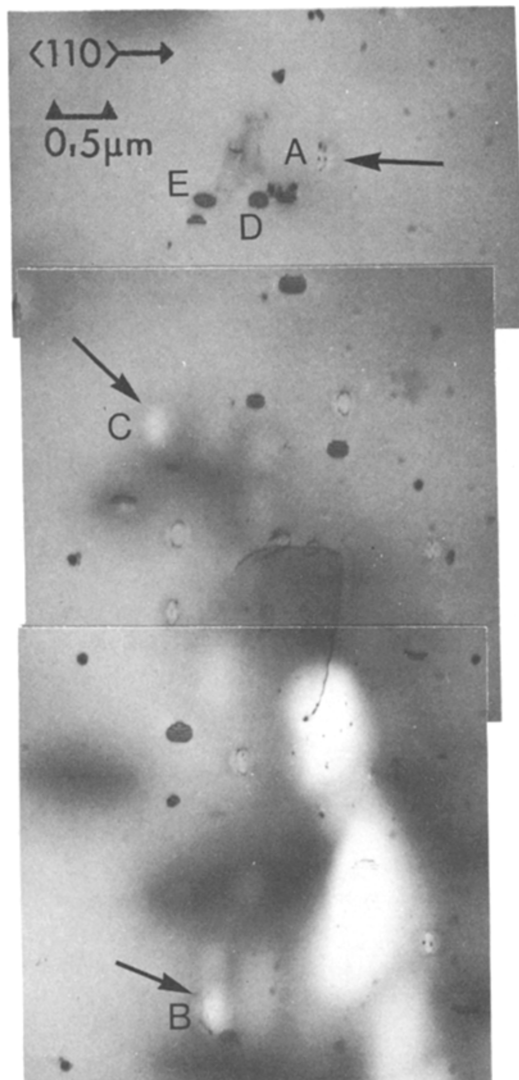

Figure 7 Stages in the development of S-pits from loop defects by A/B etching (see text for full explanation).

{1 1 1} loop also showing a "precipitate" particle, and pit C was void of any defect. It is clear that A, B and C represented S-pits at progressively later stages of attack by the etchant. This implied that the defect reponsible for pit C lay nearer to the original unetched surface than defect B, and defect B was nearer than defect A. In the central region of Fig. 7 a short length of dislocation can be seen. Comparison of Figs. 4 and 7 suggested that the dislocation in Fig. 4 was short in length because it was inclined to the {0 0 1} surface, unlike both the dislocations in Fig. 4 which lay almost parallel with the specimen surface (see Section 2.3.). At the top of the micrograph can be seen {1 1 1} loops D and E which lay within the unattacked specimen thickness.

Thus the combined A/B etched and jet-thinned TEM specimens confirm and augment the interference contrast observations, by revealing that at least some S-pits develop by etchant attack at {1 1 1} loops. It is impossible to specify directly the defects responsible for every S-pit, because the presence of an S-pit usually represents the absence of the feature which caused the pit. However, in the following sections evidence will be presented which leads to the conclusion that the majority of S-pits are due to etchant attack at loops containing "precipitate" particles.

3. Discussion

3.1. The action of the A/B etch

Previous work [10, 16, 20] used a combination of repeated etching and interference contrast microscopy coupled with repeated transmission X-ray topography of identical areas of GaAs to establish the salient features of the A/B etch behaviour. It was established that for Si-doped n-type GaAs (carrier concentration $\sim 1 \times 10^{18}\ \mathrm{cm}^{-3}$) the A/B etch generated ridges $\sim 1\ \mu$m high at dislocations. Due to a "memory-effect" the ridge structures delineating the original dislocation networks were preserved, as a two dimensional projection of the three-dimensional array, over considerable etch depth ($> 50\ \mu$m). Micrographs of the ridge structures represented the dislocation networks within the volume of material removed by the etch, and thus were somewhat analogous to X-ray transmission topographs; in particular the extent of the revealed structure was a function of the thickness of material examined (i.e. dissolved away by the etch). The present investigation of Te and Se doped GaAs has shown that for similar carrier concentrations the dislocations were not directly observed by interference contrast microscopy. Instead, their presence was revealed by the preferential attack at the various loop defects which subsequent TEM examinations showed surrounding every dislocation. This attack generated S-pits, and TEM observations have indicated that at least some of the S-pits were sited at {1 1 1} loops.

The outstanding difference between the optical and the TEM results for Te- and Se-doped specimens has been the failure of the TEM to detect reasonable densities of defects in matrix regions remote from dislocations. These regions are of considerable interest because the optical observations indicated

that etch ridges, as well as S-pits, could be found there. It is proposed that the explanation for the discrepancy is due to two connected factors; firstly the difference between "effective" sample thickness for optical requirements and TEM demands, and secondly the A/B etch memory effect. The dissolution rate of (0 0 1) GaAs material in the A/B etch is $\sim 2.5\,\mu m\,min^{-1}$ [16] so that even the shortest etch time reported here (Fig. 1a) of 85 sec duration represents a dissolved sample thickness of $\sim 3.5\,\mu m$, and for more typical etch times of 5 min the dissolved sample thickness would be $12.5\,\mu m$. The memory effect preserved defects over considerable etching distances; observations on individual S-pits such as those in Fig. 3 showed that they remained clearly identifiable by interference contrast over distances $\sim 6\,\mu m$, although as the TEM results have shown the unetched defects are only ~ 700 to 2500 Å diameter. However, the useful sample thickness for a GaAs TEM specimen is limited to $\sim 1\,\mu m$ which can perhaps be increased to $1.5\,\mu m$ by use of the HVEM. Measurements of typical S-pit densities gave values $\sim 5 \times 10^6\,cm^{-2}$. Allowing a conservative estimate of $\times$ 5 for the "effective" thickness ratio of optical to TEM requirements, the defect density expected in a TEM sample would be reduced to $\sim 10^6\,cm^{-2}$, which is in reasonable agreement with the experimental observation that few loops were detected in the matrix regions. The defect density around dislocations was $\sim 5 \times 10^8\,cm^{-2}$ from TEM observations, in reasonable agreement with a value of $\sim 2 \times 10^8\,cm^{-2}$ for S-pit density from optical micrographs.

3.2. The identification of S-pit defects

The optical micrographs of Figs. 1a and b have been discussed in detail in Section 2.2. Examination of several different specimens of Te- and Se-doped GaAs subjected to A/B etching times for as little as 30 sec to as long as 15 min have shown that Figs. 1a and b are fully representative of all the significant features. Although every region studied showed different arrangements of dislocation networks, it became apparent that every single dislocation was revealed (indirectly) in exactly the same way: as a band of close packed S-pits whose size and shape depended only on the exposure time to the etch. Occasionally, an etch ridge was observed near to the line of S-pits, but this was a rare event. In contrast, the matrix regions remote from dislocations were far less uniform across even a single specimen. Some of the regions exhibited ridge structures similar to those shown in Fig. 2, some showed only S-pits similar to those shown in Fig. 3 and others contained mixtures of S-pits and ridges in varying proportions.

Evidence from TEM observations of identical specimens has shown that the defect environment surrounding different dislocations can be different. The electron micrographs of Fig. 4 show that this difference may be due to a different number ratio of $\{1\,1\,1\}$ faulted loops to $\{1\,1\,0\}$ prismatic loops. However, all the optical evidence suggests that these two different environments will behave similarly when attacked by the A/B etch, i.e. both will become bands of close packed S-pits.

Previous work indicated that dislocations in n-type Si-doped GaAs [20] and p-type Zn-doped GaAs [21], both with carrier concentrations $\sim 1 \times 10^{18}\,cm^{-3}$ became ridge lines when A/B etched. TEM examination of dislocations in these specimens showed that the image contrast could be made zero by choice of the correct g value ($\mathbf{g} \cdot \mathbf{b} = 0$) and that no particles could be seen lying on the dislocations. It is concluded that "clean", undecorated dislocations, i.e. dislocations without "precipitate" particles, etch to give ridge structures.

The partially attacked defects (A and B) in Fig. 7 were $\{1\,1\,1\}$ loops containing "precipitate" particles, and were thin (pit) regions of the specimen. Thus it is suggested that loops etch out to become S-pits, *provided that they contain "precipitate" particles.* If they do not contain these particles, i.e. are undecorated loops, they etch as ridges. In this way the optical and TEM observations of dislocations and matrix regions can be reconciled: the defect environments surrounding dislocations will etch in a similar way provided the majority of the loops, whether $\{1\,1\,1\}$ or $\{1\,1\,0\}$, are decorated with "precipitates". It would appear that the majority of $\{1\,1\,1\}$ loops contain one or more particles; it is more difficult to detect particles at the $\{1\,1\,0\}$ loops because the loops are generally much smaller. However, it has been found from limited observations on the larger $\{1\,1\,0\}$ loops that some do, and some do not, possess "precipitate" particles. It is concluded that the majority of dislocation-associated loops are decorated in order to account for the close packed line of S-pits which delineates every optically observed dislocation. In the matrix regions both ridges and S-pits are seen; it is suggested that these indicate areas of

undecorated {1 1 0} loops and areas of decorated loops respectively.

3.3. The composition of loop defects

The loop features described in 2.3. have been seen by other workers, and almost every previous observer has put forward a different proposal for the chemical composition of the {1 1 1} loops. Abrahams *et al.* [22] found that {1 1 1} loops in VPE layers of GaAs grown with Se concentrations $4 \times 10^{19}\ cm^{-3}$ contained "opaque circles" ~ 100 to 200 Å diameter. These appeared to be similar to the "precipitate" particles described in 2.3. and 2.4. They suggested that the opaque circles were precipitates of Ga_2Se_3 and that the {1 1 1} loops were intrinsic discs of As vacancies, and/or intrinsic–extrinsic fault pairs consisting of As vacancy discs together with extrinsic loops formed from Ga interstitials. Titchmarsh and Booker [23] found that when LPE GaAs layers were grown from Sn solution on to {1 1 1} GaAs substrates, they contained large numbers of extrinsic $\frac{1}{3}\ a_0$ ⟨1 1 1⟩ dislocation loops for a doping level of $1 \times 10^{18}\ cm^{-3}$. The loop diameters ranged up to 3000 Å, and on each loop was situated a single spherical particle up to 200 Å diameter. Each particle exhibited moiré fringes, and hence was single crystal. However, it was not possible to identify the particle structure from the fringe spacing. It was suggested that particle and loop formed contemporaneously; the particle corresponded to precipitation of Sn, and the associated loop provided a means of removing Ga and As atoms from the matrix immediately surrounding the precipitate particle to allow it to grow by diffusion. Laister and Jenkins [24, 25] carried out rigorous analysis of {1 1 1} faults in heavily Te-doped GaAs (carrier concentration $> 10^{18}\ cm^{-3}$) and concluded that the faults were extrinsic, with displacement vectors of $\mathbf{R} = \frac{1}{3} a_0$ ⟨1 1 1⟩. Because the occurrence of the faults increased rapidly for both gradient freeze and Csochralski grown crystals as the carrier concentrations exceeded $10^{18}\ cm^{-3}$ it was suggested that the stacking faults must be associated with high Te concentrations, by substitution of a precipitated layer of Te atoms on As lattice sites on {1 1 1} planes. This proposal was criticised by Hutchinson and Dobson [26] on the grounds that such a substitution would not produce a sufficiently large displacement to give the observed contrast. These authors proposed that {1 1 1} faults were formed by the insertion of a layer of Ga_2Te_3, with zinc-blende structure and lattice parameter of 5.88 Å, thus producing virtually identical contrast to an inserted layer of GaAs. Since similar {1 1 1} defects were found in Se-doped GaAs it was expected that in this case Ga_2Se_3 would be formed. {1 1 0} loops seen in these materials were shown to be interstitial and unfaulted [26, 27].

Verner *et al.* [28] carefully measured displacement vector **R** values for {1 1 1} loops seen in Czochralski grown GaAs doped with Te at $\sim 10^{19}\ cm^{-3}$, after annealing treatments at 800 to 900° C. They concluded that the measured values were greater than would be expected for interstitial GaAs stacking faults, but would be consistent with a (Te + Ga) two-atom layer of spacing identical with that of {1 1 1} Ga_2Te_3 planar spacing. They assumed that this represented a stage in the decomposition of a localized supersaturated solution of Te in GaAs, the final stage being the precipitation of Ga_2Te_3 particles.

The most convincing evidence that the composition of {1 1 1} faulted loops differed from that of prismatic {1 1 0} loops was given by Hutchinson and Dobson [26]. By irradiating GaAs foils with 1 MeV electrons in a HVEM and then raising the specimen temperature to 450° C they found that the prismatic loops increased in size, presumably by absorption of interstitial Ga and As created by the irradiation. However, the faulted {1 1 1} loops in the same regions did not grow, even when the temperature was raised to 550° C, and the authors concluded that the chemical composition of the {1 1 1} loops was different. They also tentatively suggested that the "precipitate" particles present at some of the {1 1 0} loops after annealing to 380° C were due to a fast diffusing species such as copper [27].

The most recent work on defects in heavily Te-doped GaAs layers has been described by Wagner [29]. Te-doped LPE layers were grown on LPE $Al_{0.75}Ga_{0.25}As$ layers on semi-insulating (Cr-doped) GaAs substrates. The substrate and ternary were removed chemically to leave the Te-doped layer for TEM examination. For carrier concentration $> 7 \times 10^{18}\ cm^{-3}$ faulted loops with Burgers vectors characteristic of Shockley partials were found, together with pure edge dislocation loops. Most loops contained a precipitate particle, and stereomicroscopy showed that the loops always extended upwards from the precipitage towards the last-grown surface. Wagner suggested

that the dislocation loops resulted from the stress generated by the precipitation of the particles. The larger precipitates appeared to be associated with the pure edge dislocation loops, presumably because the lattice dilation they produced was sufficient to generate prismatic loops. Smaller precipitates were observed on the faulted loops, because the smaller dilation produced a shear fault.

It is clear that further work involving analytical electron microscope techniques is required in order to elucidate the compositions of both the various faulted loops which have been reported, and their attendant precipitate particles.

Acknowledgements

The authors would like to thank Birmingham University for use of their High Voltage Electron Microscope facility. Acknowledgement is made to the Plessey Company Limited for permission to publish. This work has been carried out with the support of the Procurement Executive of the Ministry of Defence and was sponsored by DCVD.

References

1. D. H. LYON, *Western Electric Engineer* 7 (1963) 3.
2. F. D. ROSI, *RCA Review* **XIX** (1958) 349.
3. A. G. TWEET, *J. Appl. Phys.* **30** (1959) 2002.
4. C. W. PEARCE and R. G. MCMAHON, *J. Vac. Sci. Technol.* **14** (1977) 40.
5. F. SECCO D'ARAGONA, *J. Electrochem. Soc.* **119** (1972) 948.
6. T. IIZUKA, *Japan J. Appl. Phys.* 7 (1968) 490.
7. *Idem, J. Electrochem Soc.* **118** (1971) 1190.
8. G. A. ROZGONYI and M. A. AFROMOWITZ, *Appl. Phys. Lett.* **19** (1971) 153.
9. G. A. ROZGONYI, T. IIZUKA and S. E. HASZKO, *J. Electrochem. Soc.* **118** (1971) 74C.
10. D. J. STIRLAND and B. W. STRAUGHAN, *Thin Sol. Films* **31** (1976) 139.
11. S. IIDA and K. ITO, *J. Electrochem. Soc.* **118** (1971) 768.
12. M. S. ABRAHAMS and C. J. BUIOCCHI, *J. Appl. Phys.* **36** (1965) 2855.
13. G. NOMARSKI and A. R. WEILL, *Rev. Metall.* (Paris) **52** (1955) 121.
14. J. G. GRADMAIER and C. B. WATSON, *Phys. Stat. Sol.* **32** (1969) K13.
15. R. W. BICKNELL, *J. Phys. D.* **6** (1973) 1991.
16. D. J. STIRLAND, Proceedings of the 6th International Symposium on GaAs and Related Compounds, Edinburgh 1976, edited by C. Hilsum (Institute of Physics, London, 1977) p. 150.
17. G. A. ROZGONYI and T. IIZUKA, *J. Electrochem. Soc.* **120** (1973) 673.
18. D. I. MAZEY, R. S. BARNES and A. HOWIE, *Phil. Mag.* **17** (1962) 1861.
19. P. B. HIRSCH, A. HOWIE, R. B. NICHOLSON, D. W. PASHLEY and M. J. WHELAN, "Electron Microscopy of Thin Crystals" (Butterworths, London, 1965) p. 165.
20. D. J. STIRLAND and R. OGDEN, *Phys. Stat. Sol.* (*a*) **17** (1973) K1.
21. D. J. STIRLAND, Unpublished results (1977).
22. M. S. ABRAHAMS, J. BLANC and C. J. BUIOCCHI, *J. Appl. Phys.* **45** (1974) 3277.
23. J. M. TITCHMARSH and G. R. BOOKER, Private communication (1975).
24. D. LAISTER and G. M. JENKINS, *Phil. Mag.* **20** (1969) 361.
25. *Idem, J. Mater. Sci.* **3** (1968) 584.
26. P. W. HUTCHINSON and P. S. DOBSON, *Phil Mag.* **30** (1974) 65.
27. *Idem, J. Mater. Sci.* **10** (1975) 1636.
28. V. D. VERNER, S. K. MAKSIMOV and D. K. NICHUGOVSKII, *Phys. Stat. Sol.* (*a*) **33** (1976) 755.
29. W. R. WAGNER, Proceedings of the 6th International Symposium on GaAs and Related Compounds, St. Louis 1976, edited by L. F. Eastman (Institute of Physics, London, 1977) p. 65.

Received 29 June and accepted 25 July 1977.